Chapter 16
LEAP-UCD-2017 Centrifuge Test at KAIST

Seong-Nam Kim, Jeong-Gon Ha, Moon-Gyo Lee, and Dong-Soo Kim

Abstract Since the earthquakes of Niigata (Japan, 1964) and Alaska (USA, 1964), the dangers of liquefaction have been highlighted and research into liquefaction has been actively performed. Particularly, as part of the provision and verification of liquefaction data through physical modeling by using centrifuge and numerical prediction, the Liquefaction Experiments Analysis Project (LEAP) was launched. The purpose of the recent LEAP-UCD-2017, in which nine facilities participated, was to evaluate the uncertainty and repeatability of response in a previous study for LEAP-GWU-2015. The ground models were prepared in a rigid box with a 5° sloping model with relative densities of 85 and 50% by using Ottawa sand. The models were subjected to nondestructive and destructive motions based on a ground motion consisting of a tapered 1 Hz sine wave. This paper describes not only the experimental procedure in detail but also the difference in the sensor response of the ground model corresponding to the relative density of 85 and 50% during liquefaction. Moreover, it provides data for permanent horizontal–vertical displacement through liquefaction and for validation of the numerical model.

S.-N. Kim
Water Management Department, Korea Advanced Institute of Science and Technology, Daejeon, South Korea

J.-G. Ha
Korea Advanced Institute of Science and Technology, Daejeon, South Korea

M.-G. Lee
Earthquake Research Center, Korea Institute of Geoscience and Mineral Resources, Daejeon, Republic of Korea

D.-S. Kim (✉)
Department of Civil and Environmental Engineering, Korea Advanced Institute of Science and Technology, Daejeon, South Korea
e-mail: dongsookim@kaist.ac.kr

16.1 Introduction

Liquefaction is a phenomenon in which the strength and stiffness of soil is reduced because of the occurrence of earthquakes or other loading. Damage and ground failure due to liquefaction remain a major concern to the geotechnical engineers. Various methods, such as field investigation and laboratory tests, have been conducted to evaluate the phenomenon and consequences of liquefaction. Simultaneously, studies involving various numerical analyses have produced various insights on liquefaction.

Constitutive models and numerical analysis techniques that simulate complex liquefaction phenomena must be validated using well-defined experimental results (Ueda and Iai 2018). Under such a demand, a collaborative study between numerical modelers and centrifuge experimenters was conducted 20 years ago, termed VELACS (Arulanandan and Scott 1993–1994). The Liquefaction Experiments and Analysis Project (LEAP) is an ongoing project to reduce the inconsistency in the experimental results and to provide high-quality experimental results to numerical modelers. In LEAP-GWU-2015, various institutions conducted the centrifuge tests on liquefaction of sloping ground in a rigid box (Manzari et al. 2015).

Following LEAP-GWU-2015, the nine facilities participated in LEAP-2017 which includes RPI, Kyoto University, KAIST, Zhejiang University, UC Davis, Cambridge University, National Central University, IFSTTAR, and Ehime University. The purpose of LEAP-2017 was to characterize the sensitivity of the liquefaction phenomena according to the relative density of the sloping ground and input motion intensity. Through centrifuge model tests, the displacement and deformation of the sloping ground were mainly evaluated, and accelerations and pore water pressure records were compared.

Researchers from KAIST developed a centrifuge facility with 5 m radius and 240 g-ton capacity in 2009, and participated in LEAP 2017. By considering the various conditions of LEAP-2017, KAIST researchers selected two cases of different relative densities (dense and loose) with the same input motion intensity of 0.15 g. This paper provides details of the centrifuge model tests conducted by KAIST for LEAP 2017, including facility and equipment, test procedure, and results.

16.2 Centrifuge Facility and Earthquake Simulator at KAIST

A dynamic geotechnical centrifuge facility at KAIST was utilized to perform tests for LEAP 2017. An electrohydraulic earthquake simulator was mounted on the centrifuge with a platform radius of 5 m and a maximum capacity of 240 g-tons. The main body of the centrifuge has the unique feature of an automatic balancing system and includes parts, such as fluid rotary joints, slip rings, and a fiber optic

Fig. 16.1 Dynamic geotechnical centrifuge facility at KAIST centrifuge testing center: (**a**) centrifuge main body, (**b**) earthquake simulator

rotary, for general testing purposes (Kim et al. 2013a). The centrifuge test of KAIST was conducted with a gravitational acceleration of 40 g.

Target excitations were applied using an earthquake simulator that adopted a dynamic self-balancing technique to eliminate a large portion of the undesired reaction forces and vibrations transmitted to the main body. The earthquake simulator was designed to operate at up to 100 g centrifugal acceleration, and the base shaking acceleration can be exerted to a maximum value of 20 g at 40 g of centrifugal acceleration with a maximum payload of 700 kg. The dimensions of the slip table were 670 mm (length) × 670 mm (width) (Kim et al. 2013b) (Fig. 16.1).

16.3 Physical Modeling

16.3.1 Soil Material and Density

Ottawa F-65 sand was used as the standard sand for LEAP-2017. The grain size characteristics and property of the soil are as follows: $Gs = 2.665$, $D_{10} = 0.13$ mm, $D_{30} = 0.17$ mm, $D_{50} = 0.20$ mm and $D_{60} = 0.21$ mm (Kutter et al. 2018). Based on the preliminary test results of the participating facilities of LEAP-2017, the minimum and maximum densities of sand were determined as $\rho_{dmax} = 1752$ kg/m^3 and $\rho_{dmin} = 1470$ kg/m^3, respectively. The target soil densities of the dense and loose centrifuge test conditions in KAIST were specified as 1703 and 1599 kg/m^3 and the relative densities were equivalent to 81% and 50%, respectively.

The sand model was constructed by dry pluviation through a screen with an opening size of approximately 1.20 mm; the screen was partially blocked to limit the flow. The density of the soil model was determined by the size of the opening slot and the drop height, and a calibration test is necessary when the geometry is
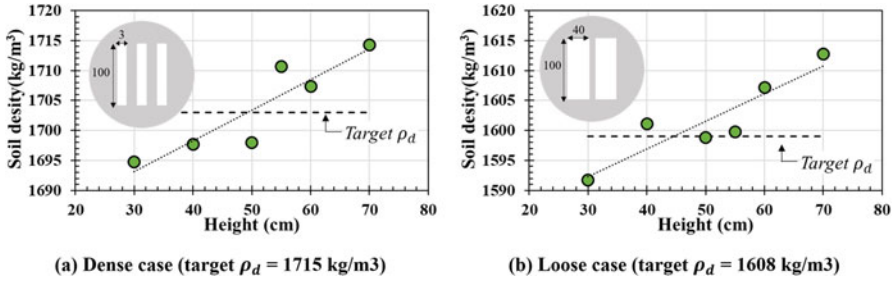
Fig. 16.2 Density versus drop height relationship for two sieve designs. (**a**) Dense case with small opening slots. (**b**) Loose case with large opening slots

changed. Figure 16.2 shows the geometry of the opening slots and the calibration test results by trial and error adjustments of the pluviation drop height for constructing the dense and loose soil models for the KAIST experiment.

The sizes of the opening slot were 3 mm × 100 mm for the dense soil and 40 mm × 100 mm for the loose soil. The drop heights in the calibration test were varied from 30 to 70 cm. From the calibration test results in shown Fig. 16.2, the final drop height was set to 55 cm in both cases.

The measured dry unit weights of soil grounds constructed in the rigid box were 1701.2 and 1592.5 kg/m³ for dense and loose conditions, respectively. After the sand was pulviated to the target height, a 5° inclined guide was installed on the top of the box. The manufactured scraper was connected directly to the inclined guide and was carefully scraped according to the slope. The soil generated by the scraping was removed as carefully as possible by using a vacuum cleaner so that the possible ground was not disturbed, and a 5° ground model was achieved.

16.3.2 Viscous Fluid

The viscous fluid was a mixture of water and methylcellulose F-65, and the target viscosity was set to 40 cSt as dictated by the scaling law defined by Garnier et al. (2007). The temperature and concentration are the influencing factors of the fluid viscosity; thus, the calibration tests were performed before model construction, as shown in Fig. 16.3. The viscosity was measured using a falling ball viscometer, which applies the Newton's law of motion under force balance when the falling spherical ball reaches its terminal velocity. The equation for calculating viscosity is expressed in Eq. (16.1) (Viswanath et al. 2007):

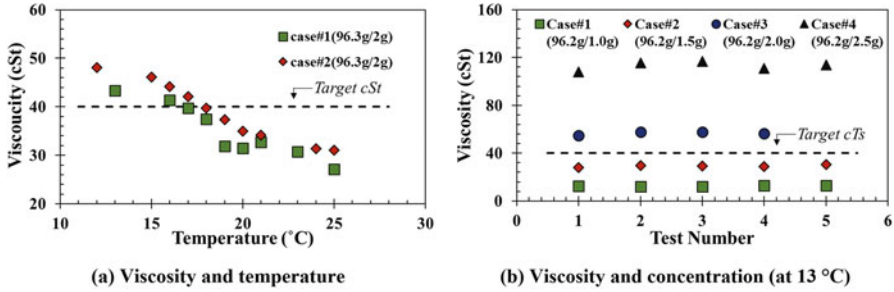$$\mu = K(\rho_{\mathrm{f}} - \rho)t, \tag{16.1}$$

Fig. 16.3 Calibration tests for viscosity according to temperature and concentration. (**a**) Viscosity and temperature. (**b**) Viscosity and concentration (at 13 °C)
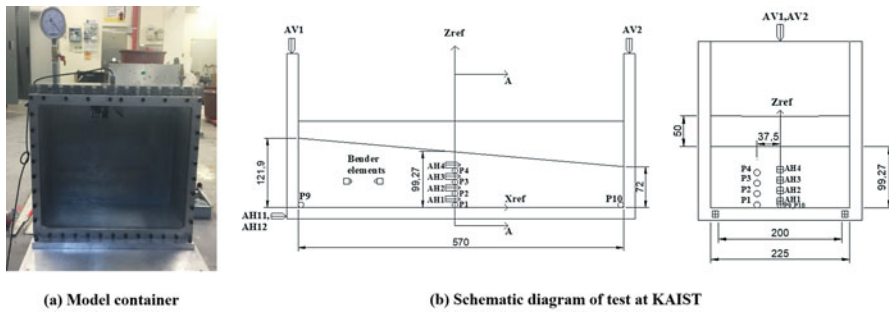

Fig. 16.4 Image of used rigid model box and the schematic of centrifuge test model and instruments. (**a**) Model container. (**b**) Schematic diagram of test at KAIST

where K is the viscometer constant, ρ_f is the ball density, ρ is liquid density, and t is the time of descent (in minutes).

At a constant concentration, the viscosity increases with the decrease in temperature (Fig. 16.3a), and the concentration increases at a constant temperature (Fig. 16.3b). The viscous fluid of the centrifuge test was prepared based on the calibration result, and the final viscosities of the dense and loose test cases were 37.45 and 35.87 cSt, respectively. These viscosities were slightly lower than the target viscosity of 40 cSt because of the sensitivity to temperature.

16.3.3   Model Description and Instrumentations

The condition for model construction in LEAP-2017 was the construction of a 5° sloping sand ground in a rigid box. A new rigid box with a transparent window was manufactured (Fig. 16.4a) with internal dimensions of 570 mm × 225 mm × 450 mm (length × width × depth). The model constructed through dry pluviation is

described in Fig. 16.4b, with the following dimensions in the prototype scale: 22.8 m × 4 m × 9 m (length × depth at midpoint × width). The length of the slope (22.8 m) was about 15% greater than the specified length (20 m). In the KAIST centrifuge facility, the 5° inclination along the length of the model was not curved because the shaking plane was perpendicular to the plane of rotation of the centrifuge. The specifications suggested that the surface should be curved in the end view (right side of Fig. 16.4b); however, the KAIST models were not curved because the error due to lack of curvature was thought to be negligible for this small model in a large centrifuge. A 4 m radius curve across the 225 width of the container would only result in about 1.5 mm elevation difference between the middle and the side of the container (75 mm in prototype scale).

The responses of the soil model during shaking were monitored using eight accelerometers along the direction of shaking (AH1–AH4 in the soil mass and AH11–AH12 on the rigid container), two vertical accelerometers (AV1 and AV2), and six pore pressure transducers (P1–P6, P9–P10). These instruments were required in LEAP-2017, and their layout is shown in Fig. 16.4. To check the variation of shear wave velocity, one pair of bender elements was installed at the same depth as that of accelerometer AH3. Table 16.1 lists the details of the instruments used.

The required 18 surface markers were installed on the ground uniformly with a spacing of 2 m × 2 m. The markers, with a diameter of 26 mm, were manufactured using PVC material and were designed to be anchored to the soil and provide minimal restriction to pore pressure drainage. A high-speed camera was mounted at the centrifuge arm to measure the plan view lateral displacements of the surface markers during shaking. The high-speed camera at KAIST is a Phantom v5.1 HI-G, which can record videos at 1200 frames per second at a resolution of 1024 × 1024 pixels. The self-balanced system of the shaking table and the hinges connecting the basket to the centrifuge arm may isolate the camera from vibrations.

16.3.4 Saturation and Container Modifications

Figure 16.5 shows the schematic of the saturation system at KAIST. Before saturating, the box was confirmed to be completely sealed from external air. The procedure for the saturation process is as follows: vacuum pressure (>94 kPa) was applied and

Table 16.1 Detailed information of instruments

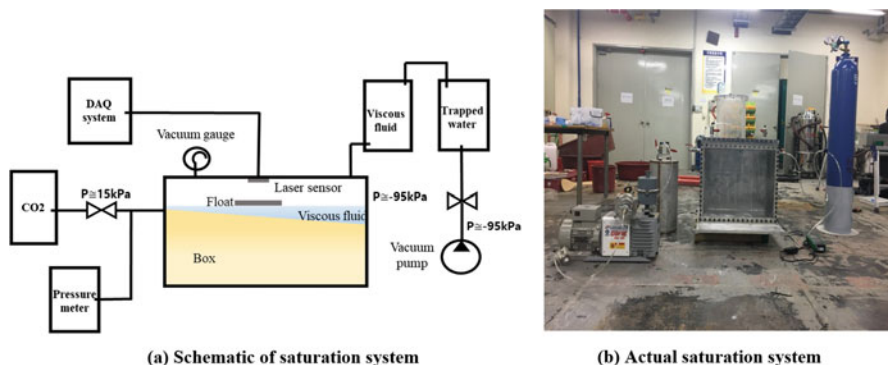| Instrument	Type	Name	Description
Accelerometer	353B17	AH1–AH4	Soil horizontal acc.
		AH11–AH12	Box horizontal acc.
		AV1–AV2	Box vertical acc.
Pore pressure transducer	PDCR 81	P1–P4	Pore water pressure in soil
	EPB-PW-3.5BS-V5/ L5M	P9–P10	Pore water pressure at boundary

Fig. 16.5 Saturation system. (**a**) Schematic of saturation system (**b**) Actual saturation system

low pressure CO_2 (<15 kPa) was flooded in the box repeatedly. This process was performed five times for 20 min each. In addition, a strong vacuum pressure was applied to eliminate the trapped air in the viscous fluid container. While maintaining vacuum pressure in the rigid box and viscous fluid container, the viscous fluid slowly dripped into the ground model (Madabhushi et al. 2018). The dripped point was in the downward direction of the slope, and to minimize the impact of gravity, sponge was installed on the ground surface. After filling the fluid up to 5 cm higher than the soil, Okamura's method was used to measure the degree of saturation (Okamura and Inoue 2012). After the rigid box was released to the atmospheric pressure, a low vacuum pressure (<15 kPa) was applied, and a change in the level of viscous fluid was observed. At this time, the volume change of the viscous fluid was the same as the volume change of the air trapped in the ground, and the degree of saturation measurement was calculated based on this result, indicating more than 99.2% and 99.4% in both models, respectively.

16.3.5 Sequence of the Centrifuge Test

Table 16.2 summarizes a typical sequence of the centrifuge tests. In each of the centrifuge tests of dense and loose ground model, four seismic excitations of two nondestructive and two destructive motions were applied. The frequency wavelets covering a wide range were used to represent the nondestructive motion to identify ground system before and after liquefaction. A tapered sine wave with a frequency of 1 Hz was designated as the destructive wave. In the KAIST tests, the target intensity was determined as 0.15 g for both the first (Motion #2) and second (Motion #3) destructive waves. By applying the destructive motions of the same intensity, the first and post liquefaction phenomena can be compared.

Cone penetration tests were conducted before and after the first destructive motion (Motion #2) to evaluate the soil condition. The cone was connected with

Table 16.2 Experimental procedure of dense and loose ground model

Event	g-level	Event description
Event #1 (CPT)	40 g	CPT (before motion)
Event #2 (seismic excitations)	40 g	Motion #1 and motion #2 (target: 0.15 g)
Event #3 (CPT)	40 g	CPT(after motion)
Event #4 (seismic excitations)	40 g	Motion #3 (target: 0.15 g) and motion #4

(a) Installation rack   (b) Cone penetration test
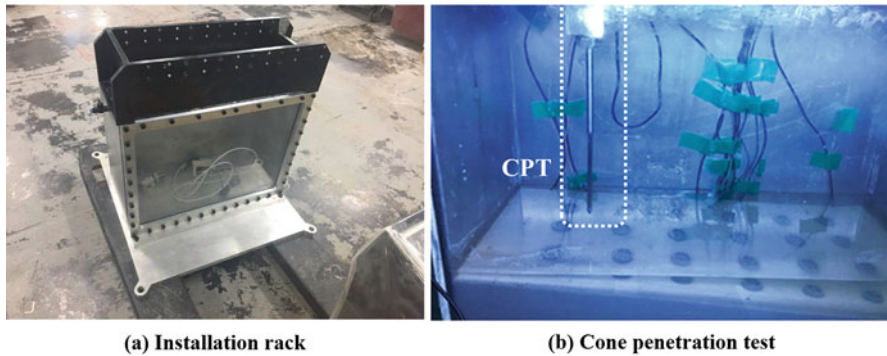
Fig. 16.6 (**a**) Rack installation onto the box. (**b**) Cone penetration test

the load cell and designed so that the strain gauge was not attached to the cone tip. The length of the cone was 200 mm, and the diameter of the cone tip was 6 mm. The penetration velocity was slow at 5 mm/s (model scale), and the penetration depth was above 75 mm (model scale). The CPTs were conducted at locations selected to avoid the sensor installed in the ground model and the marker on the ground surface. As shown in Fig. 16.6, because it was necessary to install the guide rack and loading actuator above the box for the CPT, the rotation of the centrifuge was stopped and restarted. When the centrifuge spinning was stopped, the position of the surface marker was also investigated.

16.4 Centrifuge Test Results

16.4.1 Achieved Input Motion

In the previous study, the shakers of most facilities had generated high-frequency motions superimposed on the smooth ramped sine wave motion. Therefore, the PGA_{eff} concept was introduced in the current project to attempt to compare the results among the facilities that generated different amounts of high-frequency content in the input motion:
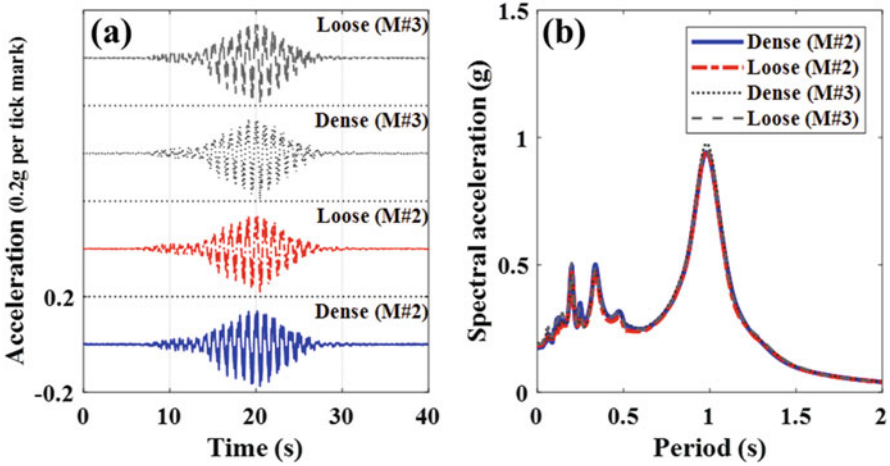
Fig. 16.7 Main input motion (Motions #2 and #3) as recorded using AH11 and AH12: (**a**) time history, (**b**) response spectrum

$$PGA_{eff} = PGA_{1Hz} + 0.5 \times PGA_{hf}, \tag{16.2}$$

where PGA_{1Hz} is a component in the frequency band of 1 Hz, and PGA_{hf} is the peak acceleration of the high-frequency components of the input motion (Kutter et al. 2018).

The main input motions (Motions #2 and #3) that were achieved for dense and loose models are shown in Fig. 16.7a. These motions were respectively measured by AH11 and AH12 accelerometers attached to the bottom side of the model box. The acceleration response spectra for the input motions presented in Fig. 16.7b show that the input motions applied to a series of tests contain some high-frequency components. However, accurately controlling the high-frequency components of the base acceleration by using the hydraulic shaker on the end of a spinning centrifuge is difficult. Therefore, compared to the deviation from the input motions of other facilities participating in LEAP-2017, the input motions applied to KAIST tests are reasonable.

Table 16.3 lists the details of main motions. The PGA_{eff} of the input motions applied in the tests were slightly higher than the target PGA_{eff} (i.e. 0.15 g).

16.4.2 Investigation of Soil Model

In the dense and loose sand models, CPT and the bender elements test (BET) were performed before and after Motion #2. The CPT results and shear wave velocity (V_s) profiles, which were deduced from the CPT results, are shown in Fig. 16.8. Here, the V_s values were derived from the method suggested from Eq. (16.3) by Kim et al.

Table 16.3 Details of main input motions applied to tests

		Target PGA$_{eff}$ (g)[a]	PGA$_{raw}$ (g)[b]	PGA$_{eff}$ (g)[c]	PGA$_{hf}$ (g)[d]	PGA$_{1Hz}$ (g)[e]	PGV (m/s)[f]	CAV$_s$ (m/s)[g]
Dense	Motion #2	0.15	0.178	0.168	0.098	0.119	0.209	7.18
	Motion #3	0.15	0.192	0.182	0.096	0.124	0.216	7.49
Loose	Motion #2	0.15	0.185	0.166	0.092	0.120	0.210	7.30
	Motion #3	0.15	0.192	0.174	0.107	0.121	0.210	7.25

[a]Targeted PGA of the 1 Hz component plus half the PGA of the higher frequency component
[b]Maximum horizontal acceleration recorded at the container base
[c]PGA of the 1 Hz component plus half the PGA of the higher frequency component
[d]PGA of the higher frequency component
[e]PGA of the 1 Hz component
[f]Peak velocity of the base input motion obtained by integration and base line correction
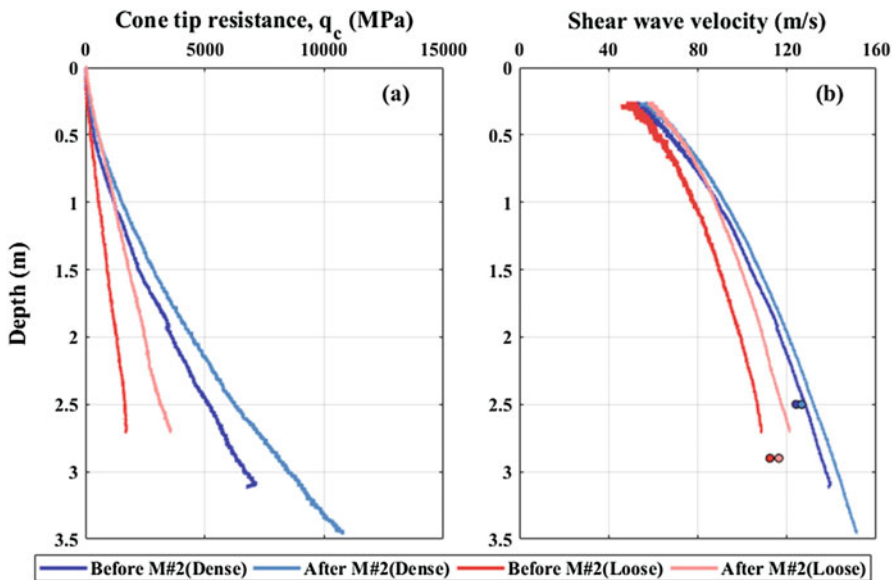[g]Cumulative absolute velocity of the base input motions with a threshold of 0.005 g (prototype)

Fig. 16.8 q_c and V_s profiles before and after Motion #2 deduced from CPT and BET results

(2017). Moreover, the V_s values obtained at a measurement depth through BET are also plotted in Fig. 16.8 for comparison, and are confirmed to be similar to those derived from the CPT results at the same depth.

The q_c and V_s values increased after Motion #2, indicating that the soil stiffness was increased by Motion #2 owing to some densification. To quantitatively present the change in the soil stiffness by Motion #2, the relative densities for each soil depth derived from the q_c profile (Kim et al. 2017) are summarized in Table 16.4. In addition, Table 16.5 describes the site periods of the soil model calculated using Eq. (16.4), in which the V_s used is converted from the CPT results:

$$V_{s1} = 125.8(q_{c1})^{0.15} \text{ (dry sand)}, V_{s1} = 108.2(q_{c1})^{0.15} \text{ (Saturated sand)} \quad (16.3)$$

$$T = 4 \sum_{i=1}^{n} \left(\frac{D_i}{V_{si}} \right) \quad (16.4)$$

where T is the site period of the soil model (s), D_i is the thickness of ith layer (m), and V_{si} is the shear wave velocity of the ith layer (m/s).

16.4.3 Excess Pore Water Pressure

Comparison of Central Array Pore Pressure Ratio with Respect to Depth

Figure 16.9 shows the response of pore pressure sensors installed in the central array at each depth. In the prototype scale, P1–P4 are excess pore water pressure response records at depths of 4, 3, 2, and 1 m, respectively. The pore pressure ratio ($R_u = \Delta u/\sigma'_{vo}$) is defined as ratio of the excess pore pressure to the initial vertical effective stress. This is generally used in liquefaction evaluation, and the liquefaction can be assumed to occur when $R_u = 1$. The black and red lines indicate the pore pressure responses in dense and loose sand, respectively. The responses of all the sensors included the generation of excess pore water pressure, generation of cycle components by dilatancy of soil during the shaking, and dissipation process after the shaking. In the dense soil condition, for the sensor closer to the ground surface, the pore pressure ratio increases and a few negative spikes occured in P4 because of dilatancy. These spikes can occur after the excess pore pressure approaches the initial effective stress and is termed as the de-liquefaction shock waves (Kutter and Wilson 1999). However, the maximum R_u value of P4 is less than 1.0, and a spike was clearly observed during the shaking, indicating that the soil behavior at a depth of 1 m is similar to that during liquefaction. In the loose soil condition, the pore pressure ratios of P2, P3, and P4 show the dilatancy spikes with the R_u value exceeding 1; thus, the liquefaction can be said to occur from the depth of 3 m based on the R_u value. However, the spikes in the positive direction occurred contrary to the negative pore pressure spikes, which was observed in the result of LEAP-GWU-2015.

Generally, it is impossible for the Ru value to exceed 1 and for the de-liquefaction shock wave to occur in the positive direction. The cause of this is presumed to be

Table 16.4 Relative densities and shear wave velocities for each soil depth derived from the CPT results

		ρ (kg/m³)	D_r	$q_{c.1.5m}$ (MPa)	D_r $(q_{c.1.5m})$	$q_{c.2.0m}$ (MPa)	D_r $(q_{c.2.0m})$	$q_{c.2.5m}$ (MPa)	D_r $(q_{c.2.5m})$
Before motion #2	Dense	1701.2	87	2.51	75	3.88	77	5.50	78
	Loose	1592.5	54	1.00	41	1.40	46	1.71	45
After motion #2	Dense	–	–	2.92	76	4.63	76	6.44	78
	Loose	–	–	1.77	59	2.45	58	3.17	57

Table 16.5 Site periods of soil model using shear wave velocity converted from the CPT results

	Before motion #2 dense	After motion #2 dense	Before motion #2 loose	After motion #2 loose
Site period (s)	0.144	0.142	0.159	0.156
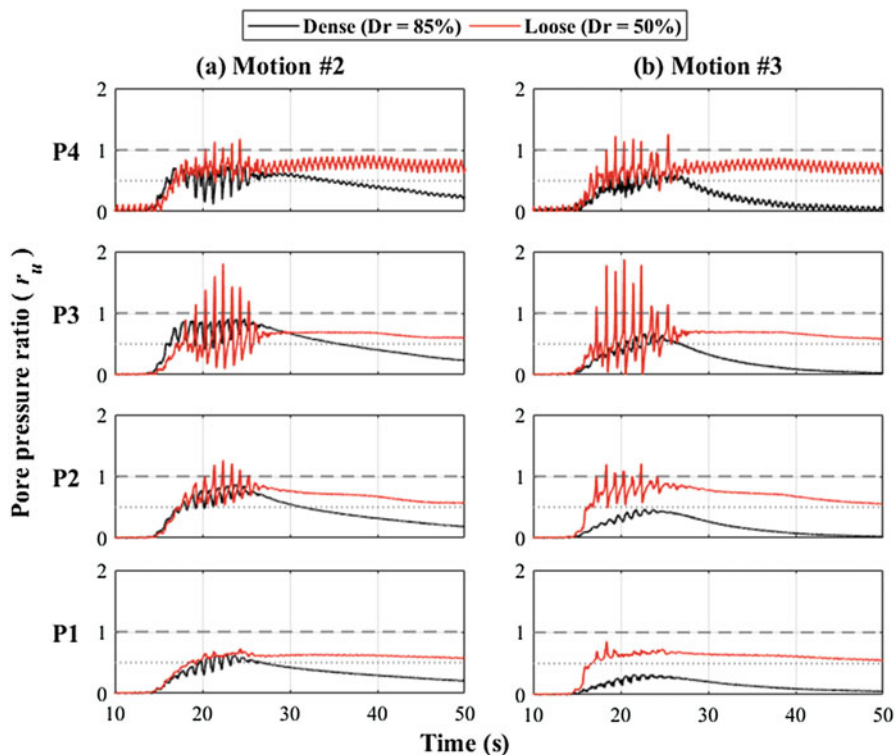
Fig. 16.9 Response of pore water pressure is divided by effective stress, and represented according to the time histories at specific depth by pore pressure ratio (Black and red lines represent the responses of the dense and loose models, respectively): (**a**) Motion #2, (**b**) Motion #3

local dynamic compressive stress around sensors due to sensor installation and hand pluviation. Also sensors wire stiffness may be somewhat affecting the response.

Sensor P2 dissipated immediately after the earthquake at approximately 30 s. Therefore, the presence or absence of liquefaction based on the depth should be examined from other aspects also. Unlike P2, P3, and P4, P1 is installed at the bottom of the box and is not surrounded by sand in all directions, thus it has a relatively low cyclic response.

The pore pressure ratios in the dense soil condition during Motion #3 are described in Fig. 16.9b, which shows not only the overall low pore pressure ratio but also faster dissipation rate than that of Motion #2. In case of the loose soil

condition during Motion #3, similar responses were generated as those in Motion #2; however, the spike shapes were slightly changed asymmetrically. This may be because the void ratio of soil decreased in both cases, and because the geometry of the sloping ground was changed by the movement from the previous shaking in Motion #2.

Dissipation Time of Pore Pressure

Figure 16.10 shows the variations in excess pore water pressures of the central array with respect to time according to the soil relative density and main input motion. Figure 16.10a-1 and b-1 show response graphs in the dense and loose models when Motion #2 is imposed on the ground model. Similarly, Fig. 16.10a-2 and b-2 show response graphs when Motion #3 is imposed on the ground model.

In Fig. 16.10a-1 and b-1 displaying Motion #2, the excess pore water pressure, which was measured at a deeper depth, appeared higher and was dissipated at the end of the motion (28 s). The dissipation time in the loose model was longer than that
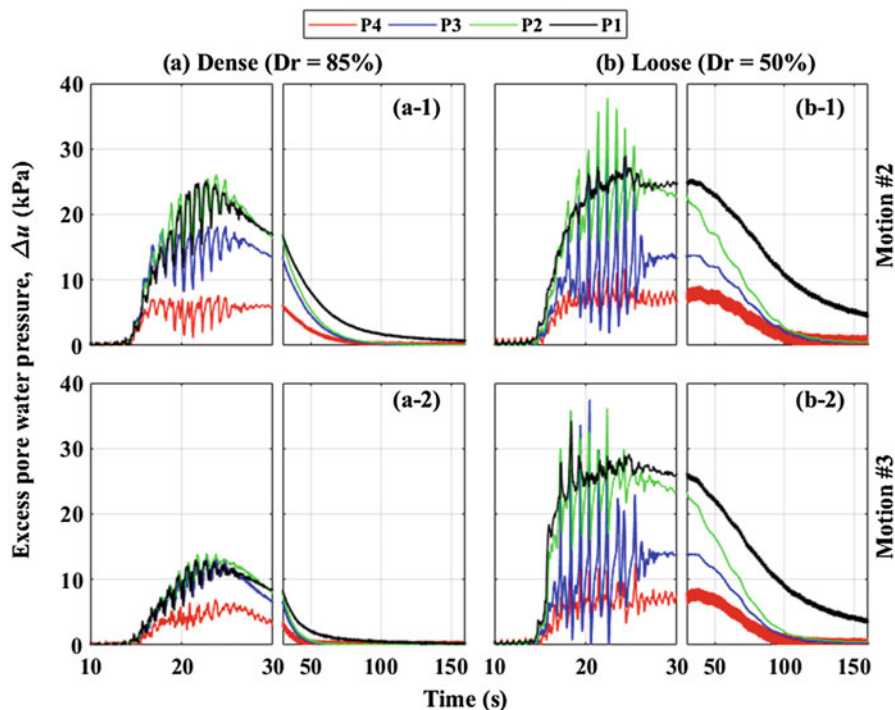
Fig. 16.10 Excess pore water pressure data with respect to the depth of main input motion (Motions #2 and #3). P1, P2, P3, and P4 are the pore water pressure responses at depths of 4, 3, 2, and 1 m, respectively. (**a-1**) Motion #2 of dense model, (**a-2**) Motion #3 of dense model, (**b-1**) Motion #2 of loose model, and (**b-2**) Motion #3 of dense model

in the dense model. Almost all the excess pore water pressure was dissipated at 150 s in the dense model; however, the dissipation in the loose model took more than 150 s. In Fig. 16.10a-2 and b-2, showing the imposition of Motion #3, the dissipation rate patterns accelerated because of the change of void ratio and permeability following liquefaction.

Effect of Radial Gravity Field on P9 and P10

Figure 16.11 shows the results of time histories P9 and P10 installed in the side boundary of the rigid box (Hung et al. 2018). The figure shows the characterization of the radial gravity field generated by the change in the g-level while conducting the spinning centrifuge test. P9 and P10 are located at a position where the water level is relatively lower than P1 during spinning. As shown in Fig. 16.11, the pore pressure responses of P9 and P10 are smaller than that of P1. Similar with LEAP-GWU-2015 results, all facilities in LEAP-2017 showed this trend.

16.4.4   Acceleration Responses

Comparison of Central Array Accelerations Based on Depth

Figure 16.12 shows the acceleration time histories when Motion #2 is applied to the ground model. The black and red lines represent the acceleration responses in the dense and loose models, respectively, and the depths from AH1 (4 m) to AH4 (1 m
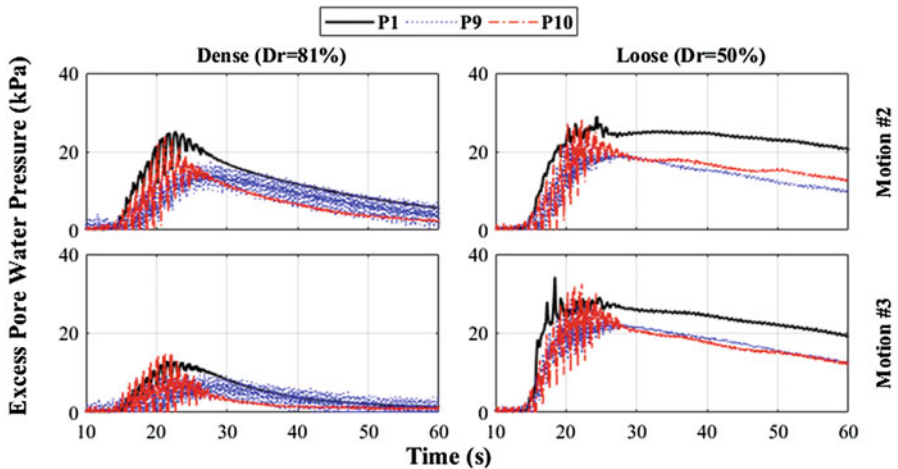

Fig. 16.11 Comparison of excess pore water pressure of P1, P9, and P10. Verification of water level change due to radial gravity field during rotation of centrifuge
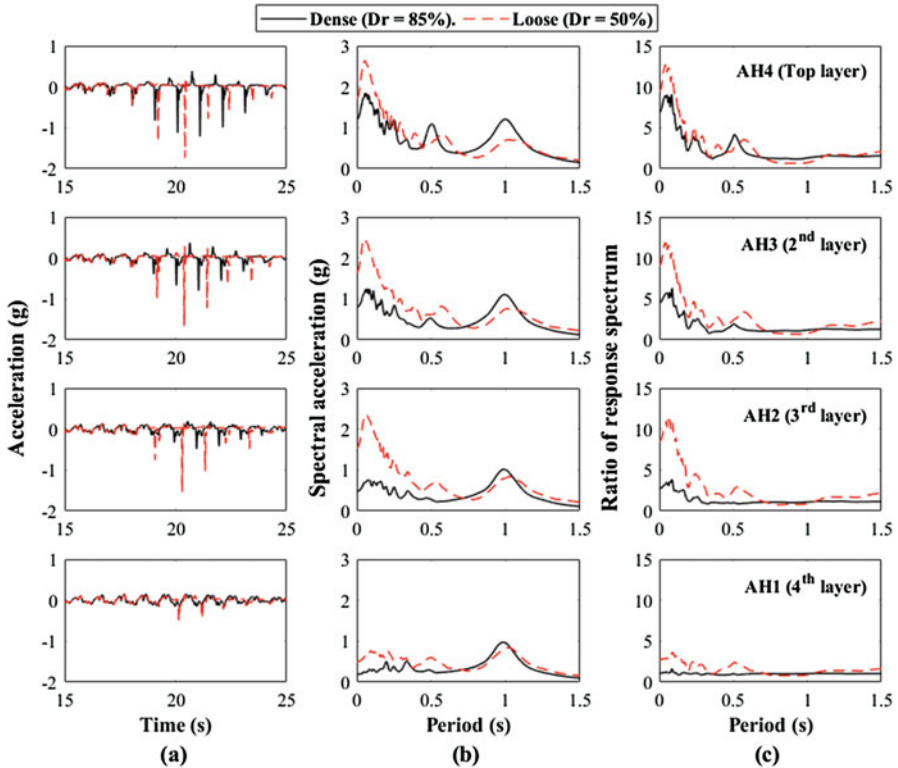
Fig. 16.12 Acceleration response recorded with respect to depth when Motion #2 of target PGA of 0.15 g was applied to the ground model. The black and red lines indicate the responses of acceleration for the dense and loose models, respectively. Graphs of (**a**) acceleration, (**b**) response spectrum, and (**c**) ratio response spectrum with respect to time

deep) are continuously increased by 1 m. Figure 16.12a on the left shows the occurrence of spike due to soil dilatancy, caused by a de-liquefaction shock wave. The sharp spike in the dense model began to appear gradually at a depth of 3 m (AH2) but occurred from the depth of 4 m (AH1) in the loose model. In addition, the closer to the ground surface, the more the spike is amplified. This response is presented asymmetrically owing to the sloping ground model.

Figure 16.12b shows the response spectrum with respect to depth based on the measured acceleration record. The spectral acceleration tend to increase at approximately 0.1, 0.5, and 1 s. In the loose model, at approximately 0.1 s, the spectral acceleration response was larger than that in the dense model. This is because the de-liquefaction shock wave, which is a high-frequency component, was larger in the loose model. Moreover, for the loose model, the peak in the response spectrum near 1 s period was observed to increase above 1 s.
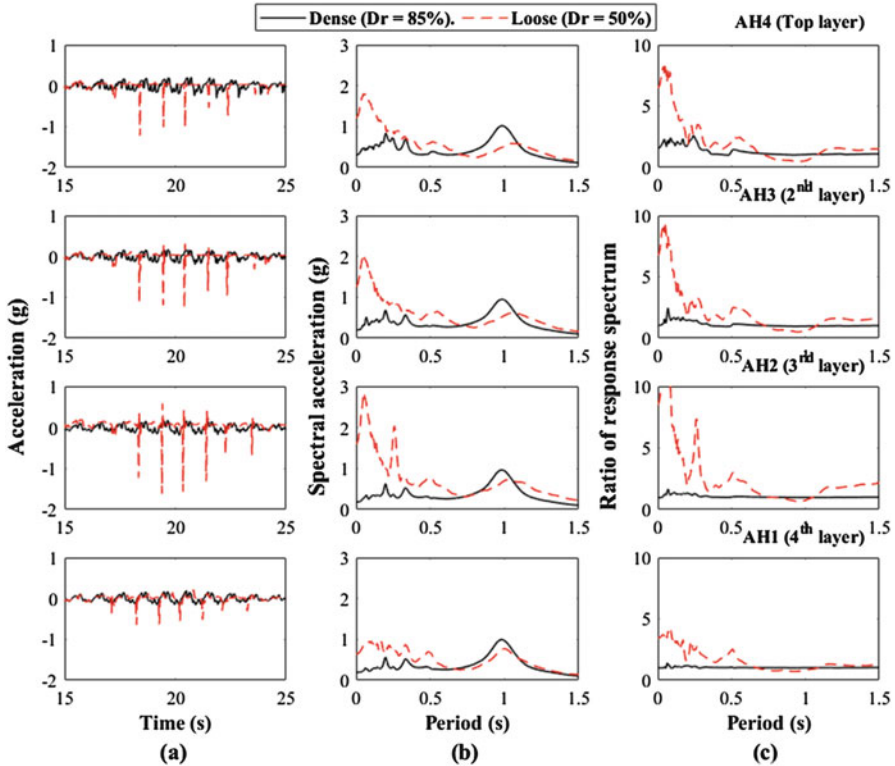
Fig. 16.13 Acceleration response recorded with respect to depth when Motion #3 of target PGA of 0.15 g was applied to the ground model. Black and red lines indicate the responses of acceleration in the dense and loose models, respectively. Graphs of (**a**) acceleration, (**b**) response spectrum, and (**c**) ratio response spectrum with respect to time

The ratio of response spectrum in Fig. 16.12c is defined as the ratio of the response spectrum of the ground to the input motion measured by AH11 and AH12. This ratio is considerably similar to the trend of the response spectrum in Fig. 16.12b, except for the response near 1 s.

Figure 16.13 shows the acceleration response when Motion #3 is imposed on the model. In Fig. 16.13a, the spike due to soil dilatancy did not appear in the dense model. This implies that the relative density increases during the ground consolidation after application of Motion #2. Table 16.4 presents the quantitative values. In the loose model, the spike still occurred at all depths but was relatively smaller, and the occurrence phase became faster compared with the acceleration response of Motion #2. Figure 16.13b are response spectra, showing the same tendency as in Motion #2. Compared with Motion #2, the peak point at approximately 0.1 s for Motion #3 was relatively small in both models. This is also presumed to increase the relative density of the ground due to the soil consolidation. Therefore, the ratio response spectrum Fig. 16.13c was also smaller when compared with that in Motion #2 near 0.1 s.
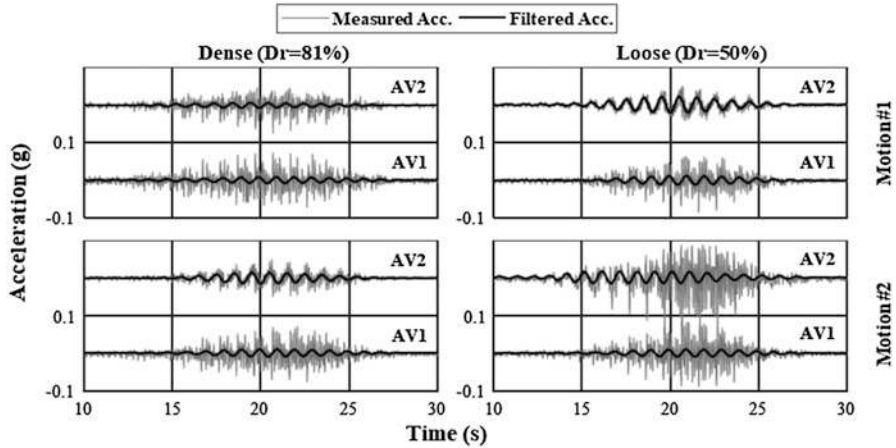
Fig. 16.14 Vertical acceleration record measured using AV1 and AV2 for verifying the rocking effect. The black lines represent raw data, while the gray lines show the 0.3–3 Hz band pass filtered data

Vertical Acceleration of the Rigid Box from AV1 and AV2

Figure 16.14 shows the rocking behavior measured using AV1 and AV2 accelerometers installed at the top and outside of the box. The gray lines indicate the unfiltered motions and the black lines represent the filtered band pass to show the components of motion between 0.3 and 3 Hz. Due to the rocking effect, an overturning moment can be induced by the inertial force between the ground model and box, and can be amplified by the resonance frequency.

The vertical acceleration has a peak, which is far lower than that in the base input motion, and AV1 (the upslope side of the model) and AV2 (the downslope side of the model) are asymmetrical in the loose model. The rocking accelerations are expected to be of the opposite sign (180° out of phase) for AV1 and AV2 (Kutter et al. 2018). Based on the measured acceleration, the rocking effect was seen because the phase difference of the two vertical accelerometers was contradictory in Motion #2. The results of Motion #3 show the rocking effect due to the asymmetric acceleration records AV1 and AV2, and future research is needed to determine how this rocking effect will affect the liquefaction behavior.

16.4.5 Comparison Between Acceleration and Pore Water Ratio

Figure 16.15 shows the superimposed acceleration and pore pressure ratio time histories. This figure shows that the spike of the acceleration record, which is the
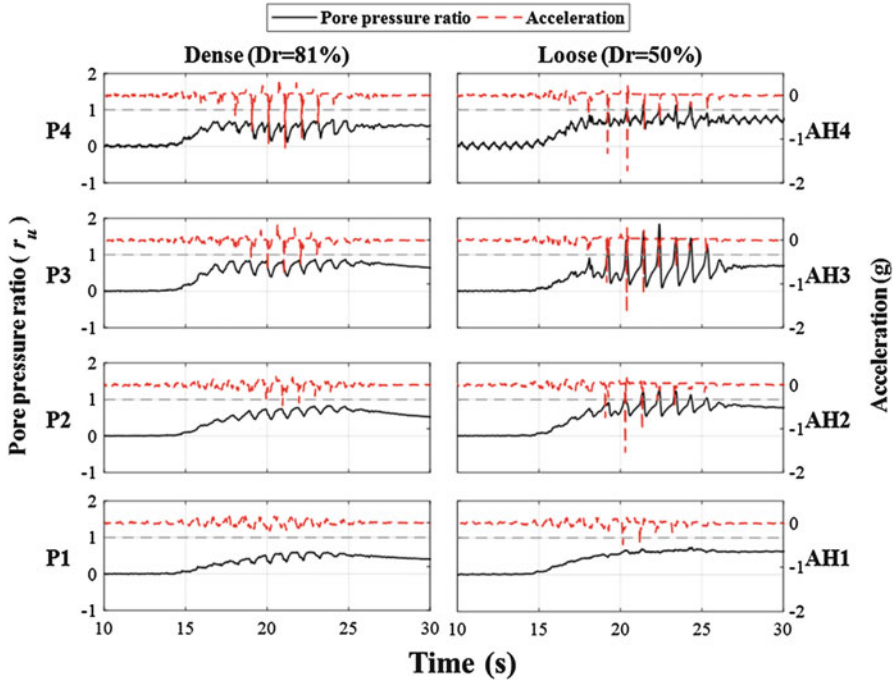
Fig. 16.15 Acceleration and pore water ratio records superimposed by depth

de-liquefaction shock wave, coincides with the pulse where the excess pore water pressure is temporarily reduced. Such a phenomenon can be seen at the depth of AH4, with P4 installed on the ground surface of the dense model. In the loose model, the de-liquefaction shock wave appeared from P2 at the AH2 depth.

De-liquefaction is described as the temporary solidification of soil caused by dilatancy at large shear strains, and re-liquefaction is described as the return to a state with effective stress of zero due to the unloading of the shear stress (Kutter and Wilson 1999). That is, the spike pulses in the acceleration record coincide with pulses of negative pore pressure; this is called the de-liquefaction shock wave.

As shown in Fig. 16.15, the point of occurrence of the de-liquefaction shock wave in the loose model differs for each depth. For the depth of AH4, P4 is closest to the ground surface and the de-liquefaction shock wave occurred in approximately 17 s. In contrast, it occurred at approximately 18 s at the AH3 depth for P3. Moreover, it was generated at 24 s in AH2 for P2. The deeper it is from the ground surface, the more the generation time of the spike is delayed.
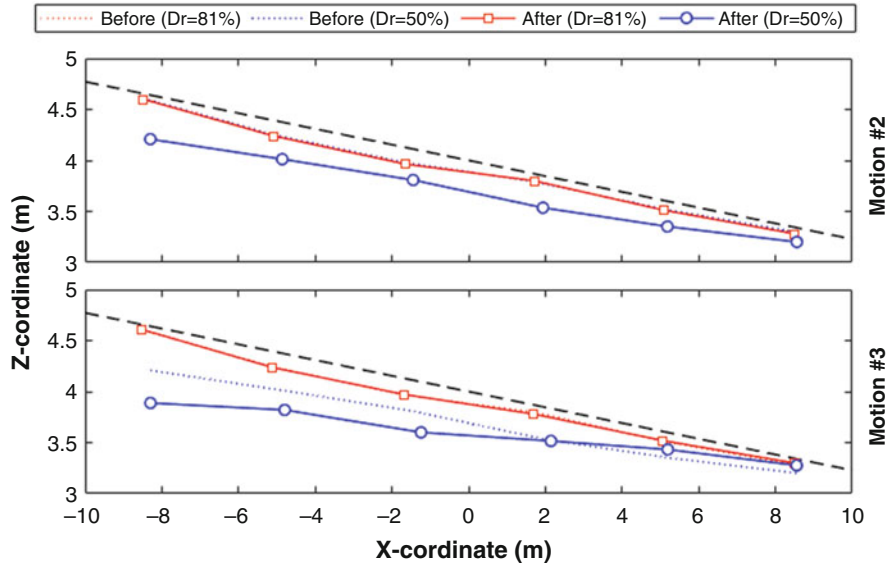
Fig. 16.16 Measurement is executed at 1 g-level after completely stopping the centrifuge operation, and vertical displacement was measured directly from the front of the box (Dashed, red, and blue lines represent displacement of original ground model, dense model, and loose model, respectively)

16.4.6 Displacement of Surface Marker

Comparison of Vertical Displacement

Figure 16.16 shows the measured vertical displacements of loose and dense ground models after Motions #2 and #3. The vertical displacement measurement was performed at 1 g after complete stopping of the centrifuge, and the displacement was directly measured from the front of the box according to the markers position. The dashed line represents the original ground model before motion was applied, and the geometries of both models were the same. The red and blue lines show the change in the vertical displacement of the dense and loose models, respectively, after the shakings.

When Motion # 2 was imposed on the model, vertical displacements of 9 and 223 mm were generated in the dense and loose models, respectively, at the prototype scale. In the dense model, almost no vertical displacement occurred compared to that in the loose model. As shown in Fig. 16.16, the vertical settlements in Motion #3 were smaller in both models compared to those in Motion #2. The dense model had showed a slight change in displacement, while the loose model produced an overall 97 mm (prototype) displacement. This implies that the relative density of the ground increased after Motion #2. In the loose model, the vertical settlement at the lower slope near the x-coordinates of 5–8 m was negative, because it is assumed that the sand of the upslope part drifted down, and the ground level was raised.
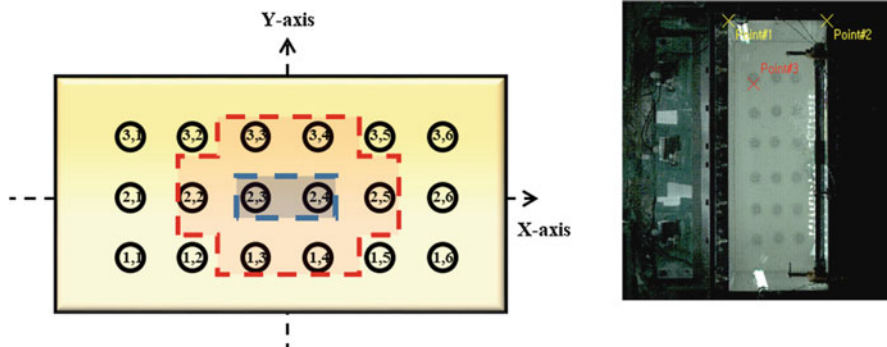
Fig. 16.17 Surface markers coordinate system (the markers included in the red line have a relatively large permanent horizontal displacement) and TEMA software sets the points (points #1 and #2 are the reference points and point #3 is the tracking point)

Comparison of Horizontal Displacement

The TEMA software was used to track targets and measure horizontal displacement of the makers based on the saved video. Before using this tool, the box width was fixed with two reference points, and the actual length was set by entering it. Actually, the box width was 225 mm and was scaled according to this length; the displacement was calculated by tracking the displacement of the marker. Figure 16.17 shows the reference points (points #1 and #2) and marker tracking point (point #3). After measuring the reference points of the width of the box to the scaling points, a permanent horizontal displacement, which was tracked by a marker point, was detected in real time. To achieve high-quality displacement results, a lighting system was built by installing LEDs on the rigid box.

Figure 16.18 shows the typical time histories of horizontal displacements obtained using the TEMA software. Permanent displacements during shaking are shown with respect to the time histories. The measured time was longer than the displayed time but was terminated at 40 s because of the difficulty in accurately measuring displacement due to water wave. It is recommended to install the thick cover plate presented in the LEAP guideline to minimize the water wave.

The changes in horizontal displacement before and after Motions #2 and #3 for the dense and loose models are shown in Fig. 16.19 through contour lines. Figure 16.17 shows a total of 18 surface markers installed on the ground surface, and the red part indicates the center markers where the displacement occurred relatively more than at other points. The contour line was presented by tracking the horizontal displacement for each marker during shaking. Notably, there was hardly any occurrence of displacement in the dense model. In contrast, in the loose model, the markers moved on average in the downslope direction by 134 mm (prototype). Especially, the horizontal displacement of the markers installed in the middle slope was 169 mm (prototype), which is higher than the average. A special point is that the displacement of the first horizontal marker line tends to occur significantly.
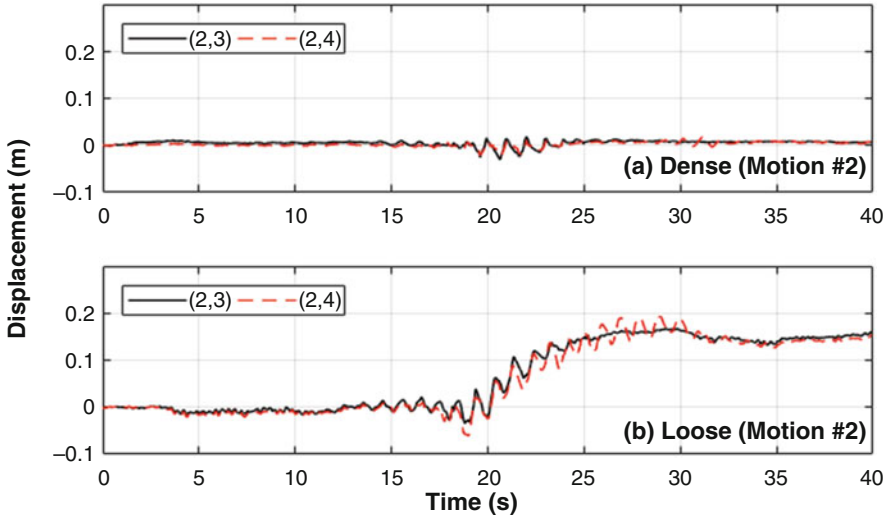
Fig. 16.18 Representative results tracking the permanent horizontal displacement of markers by using TEMA software. Permanent horizontal displacement of the dense model hardly occurs, and approximately 200 mm occurs in the loose model
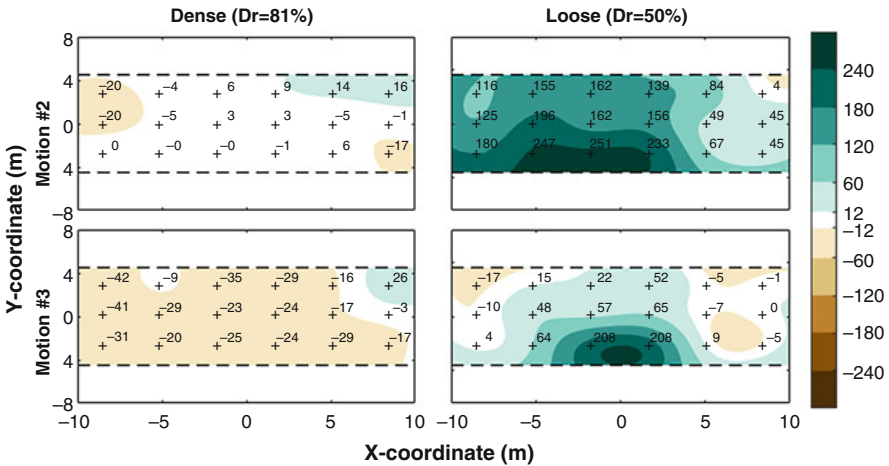

Fig. 16.19 Contour line is presented using calculation of the horizontal displacement for each marker by using TEMA software

In this part, as the front of the box, the contact between the front part of the acrylic material and the soil particles makes the friction force smaller than the other parts. Therefore, there is possibility that a larger horizontal displacement may occur compared with other parts. The horizontal displacement of the markers placed at

the other edge of the box was suspected to be smaller than other markers owing to the boundary effect.

The amount of displacement after Motion #3 is 50% or smaller than the displacement after Motion #2. Since a considerable amount of time passed after Motion #2, the ground stiffness is suspected to increase due to the rearrangement of particles. As shown in Table 16.4, relative density was measured through the CPT after Motion #2, and it is found that the relative density increased. Therefore, even with a similar PGA in Motion #3, the horizontal displacement occurred in both models was slight. However, the marker horizontal displacement of the dense model seemed to be moved toward the upslope direction. This reflects the difficulty of the accurate measurement by water wave (Kokkali et al. 2018).

16.5   Conclusion

Facilities in each country participated in LEAP-2017, and the same sand, viscous fluid, type of input motion, and box conditions were used to ensure data reliability. However, the relative density of the soil and the input motion intensity were set as variations and the liquefaction behavior by these two variations was evaluated. KAIST evaluated the liquefaction behavior at two different densities: a dense model ($D_r = 85\%$) and loose model ($D_r = 50\%$). Two destructive motions with amplitude of about 0.15 g (Motions #2 and #3) were applied to both models. By participating for the first time in this project, KAIST performed physical modeling by using a technical method described in the LEAP guidelines. The technical method for the liquefaction experiment was described in detail in Sect. 16.2.

There are three important results of this project: response of pore pressure, response of acceleration, and displacement.

1. De-liquefaction shock wave occurred in pore pressure response, and the spikes in the loose model were larger than that in the dense model. In addition, the dissipation time of the excess pore water pressure was relatively greater in the loose model.
2. In the acceleration response, a de-liquefaction shock wave occurred largely in the loose model. The spectral accelerations of the ground motions show the frequency content of the input motion and the de-liquefaction shock waves.
3. As a result of the displacement, vertical and horizontal displacements occurred in the loose model. In particular, the displacement of the markers near the center of the ground was relatively larger than the displacement of the markers located at the edge. This phenomenon was caused by the boundary conditions imposed by the rigid model container.

Both Motions #2 and #3 have the same input motion component and PGA. The comparison of the response to these motions showed that the responses of acceleration, pore water pressure, and displacement indicated less nonlinearity during Motion #3 than Motion #2. Densification or strengthening of the models is also

consistent with the increase in cone penetration resistance due to applying Motion #2 before Motion #3.

As an organization that participated in LEAP project for the first time, there are some suggestions for the betterment of the project; this includes technical limitation and difficulties of KAIST while experimenting.

1. In the course of the creating of the ground model, there was a great difficulty in installing sensors. The line of the sensor is not flexible, and it is difficult to place the sensor at the accurate position. This may lead to ground disturbances and cause the relative density per layer to be asymmetric. Therefore, it is important to think about how you can safely and accurately position the sensor installation.
2. There was an insufficient quantity of light, an insufficient contrast of markers, and an error disturbing accurate measurement with respect to water wave in measuring displacement. If these problems are solved, better quality data could be extracted.

References

Arulanandan, K., & Scott, R. F. (1993). *Verification of numerical procedures for the analysis of soil liquefaction problems*. Brookfield: A.A. Balkema.

Garnier, J., et al. (2007). Catalogue of scaling laws and similitude questions in geotechnical centrifuge modelling. *International Journal of Physical Modelling in Geotechnics, 7*(3), 1.

Hung, W.-Y., Lee, C.-J., & Hu, L.-M. (2018). Study of the effects of container boundary and slope on soil liquefaction by centrifuge modeling. *International Journal of Soil Dynamics and Earthquake Engineering, 113*, 682–697. https://doi.org/10.1016/j.soildyn.2018.02.012.

Kim, D.-S., et al. (2013a). A newly developed state-of-the-art geotechnical centrifuge in Korea. *KSCE Journal of Civil Engineering, 17*(1), 77–84.

Kim, D.-S., et al. (2013b). Self-balanced earthquake simulator on centrifuge and dynamic performance verification. *KSCE Journal of Civil Engineering, 17*(4), 651–661.

Kim, J.-H., Choo, Y. W., & Kim, D.-S. (2017). Correlation between the shear-wave velocity and tip resistance of quartz sand in a centrifuge. *Journal of Geotechnical and Geoenvironmental Engineering, 143*(11), 04017083.

Kokkali, P., Abdoun, T., & Zeghal, M. (2018). Physical modeling of soil liquefaction: Overview of LEAP production test 1 at Rensselaer Polytechnic Institute. *Soil Dynamics and Earthquake Engineering, 113*, 629–649.

Kutter, B., Carey, T., Hashimoto, T., Zeghal, M., Abdoun, T., Kokalli, P., Madabhushi, G., Haigh, S., Hung, W.-Y., Lee, C.-J., Iai, S., Tobita, T., Zhou, Y. G., Chen, Y., & Manzari, M. T. (2018). LEAP-GWU-2015 experiment specifications, results, and comparisons. *International Journal of Soil Dynamics and Earthquake Engineering, 113*, 616–628. https://doi.org/10.1016/j.soildyn.2017.05.018.

Kutter, B. L., & Wilson, D. W. (1999). De-liquefaction shock waves. In: *Proceedings of the seventh US–Japan workshop on earthquake resistant design of lifeline facilities and countermeasures against soil liquefaction* (p. 295–310). Seattle.

Madabhushi, S. S. C., Haigh, S. K., & Madabhushi, G. S. P. (2018). LEAP-GWU-2015: Centrifuge and numerical modelling of slope liquefaction at the University of Cambridge. *International Journal of Soil Dynamics and Earthquake Engineering, 113*, 671–681. https://doi.org/10.1016/j.soildyn.2016.11.009.

Manzari, M. T., Kutter, B. L., Zeghal, M., Iai, S., Tobita, T., Madabhushi, S. P. G., Haigh, S. K., Mejia, L., Gutierrez, D. A., & Armstrong, R. J. (2015). LEAP projects: concept and challenges. In *Proceedings of the fourth international conference on geotechnical engineering for disaster mitigation and rehabilitation*. (4th GEDMAR), 2014 Sept 16–18. Kyoto: Taylor & Francis.

Okamura, M., & Inoue, T. (2012). Preparation of fully saturated models for liquefaction study. *International Journal of Physical Modelling in Geotechnics, 12*(1), 39–46.

Ueda, K., & Iai, S. (2018). Numerical predictions for centrifuge model tests of a liquefiable sloping ground using a strain space multiple mechanism model based on the finite strain theory. *International Journal of Soil Dynamics and Earthquake Engineering, 113*, 771–792. https://doi.org/10.1016/j.soildyn.2016.11.015.

Viswanath, D. S., et al. (2007). Introduction. In *Viscosity of liquids* (pp. 72–80). Amsterdam: Springer.